Evidence of a gravity wave breaking event and the estimation of the wave characteristics from sodium lidar observation over Fort Collins, CO (41°N, 105°W)

Tao Li,[1,2] C.-Y. She,[1] Han-Li Liu,[3] and Michael T. Montgomery[4,5]

Received 9 December 2006; accepted 15 February 2007; published 10 March 2007.

[1] On the night of December 3rd, 2004 (UT day 338), we observed a significant acceleration of horizontal wind near 100 km between 0900 and 0915 UT accompanied by a temperature cooling at the same altitude and warming below it. The Lomb spectrum analysis of the raw dataset revealed that a gravity wave with 1.5 hr period was significant between 0500 and 0900 UT, but blurred after 0900 UT, suggesting the transfer of wave energy and momentum from wave field to mean flow. Most likely, this observed phenomenon is due to the breaking of an upward propagating gravity wave with an apparent period of ~1.5 hr. Using linear saturation theory and assuming a monochromatic wave packet, we estimated the characteristics of breaking gravity wave, eddy diffusion coefficient, and a simple relation between Prandtl number and turbulence localization measure when the wave is breaking, from the experimentally determined heating rate, horizontal wind acceleration, and background temperature and winds. **Citation:** Li, T., C.-Y. She, H.-L. Liu, and M. T. Montgomery (2007), Evidence of a gravity wave breaking event and the estimation of the wave characteristics from sodium lidar observation over Fort Collins, CO (41°N, 105°W), *Geophys. Res. Lett.*, *34*, L05815, doi:10.1029/2006GL028988.

1. Introduction

[2] Atmospheric gravity waves, since first observed and studied in the ionosphere by *Hines* [1960], have been a major research topic for many decades because of their dramatic impacts on the energy and momentum budgets in the middle and upper atmosphere [*Fritts and Alexander*, 2003]. Because the wave energy density is constant for a gravity wave propagating energy upward, the amplitude of the wave grows with altitude to compensate the exponential decease of air density. In the mesopause region (80–105 km), the gravity waves could become unstable and tend to break via either convective or dynamic instability, and thus turbulence is generated within the wave field [*Fritts and Rastogi*, 1985]. The breaking gravity wave will deposit momentum into the mean flow and induce vertical heat flux, leading to wind acceleration/deceleration and temperature changes around the breaking region [*Lindzen* 1981; *Liu and Hagan*, 1998].

[3] In recent years, many gravity wave breaking cases were studied with the temperature vertical profiles observed by Rayleigh lidar [*Hauchecorne et al.*, 1987; *Meriwether et al.*, 1998] and sodium lidar [*Williams et al.*, 2002]. But there are very few publications on the gravity wave breaking revealed by simultaneous observations of both temperature and horizontal wind with high vertical and temporal resolutions. The Colorado State University (CSU) sodium lidar system located in Fort Collins, CO (40.6°N, 105°W) is one of the most robust ground-based lidar systems and is capable of simultaneously observing temperature and horizontal wind in the mesopause region on a 24-hour continuous basis, weather permitting. Many valuable datasets have been collected under this operational mode since May 2002 [*She et al.*, 2004]. In this paper, we present lidar data from the night of December 3rd, 2004, and the observation of a large sudden horizontal wind acceleration near 100 km accompanied by a temperature change implicating a sudden downward heat flux transport. These observed features are highly suggestive of wave breaking in these altitudes. With the observed heating rate and wind acceleration, we estimated the characteristics of the breaking gravity wave, using the linear saturation theory. The estimated parameters are consistent with an observed wave with a period of ~1.5 hr, whose spectrum power was greatly reduced after the sudden horizontal wind acceleration and temperature cooling near ~100 km and warming below it. Discussions will be presented followed by a conclusion.

2. Sodium Lidar Observations

[4] The CSU sodium lidar system currently utilizes a three-frequency design that enables simultaneous observations of temperature, zonal wind, meridional wind and sodium density in the mesopause region on a 24-hour continuous basis. The system receiver employs two 14-inch Celestron telescopes pointing eastward and northward, both at 30° from zenith. The lidar transmitter directs two laser beams into the atmosphere, each aligned parallel to one telescope, with north and east beams separated by ~70 km in the mesopause region. In comparison to other lidar systems, our sodium lidar system has a modest power-aperture product of 0.05 Wm^2 per beam. However, due to the resonance enhancement in laser induced fluorescence, the received signal is sufficient to probe atmospheric instabilities as well as various atmospheric waves and their interactions [*She et al.*, 2004; *Li et al.*, 2005]. The precision of the measurements for temperature and wind with a 2 km vertical resolution and 15 min temporal resolution under the nighttime clear sky condition is estimated to be

[1]Department of Physics, Colorado State University, Fort Collins, Colorado, USA.
[2]Now at Table Mountain Facility, Jet Propulsion Laboratory, California Institute of Technology, Wrightwood, California, USA.
[3]High Altitude Observatory, National Center for Atmospheric Research, Boulder, Colorado, USA.
[4]Department of Meteorology, Naval Postgraduate School, Monterey, California, USA.
[5]Hurricane Research Division, NOAA, Miami, Florida, USA.

0094-8276/07/2006GL028988$05.00

Report Documentation Page

Form Approved
OMB No. 0704-0188

1. REPORT DATE	2. REPORT TYPE	3. DATES COVERED
MAR 2007		**00-00-2007 to 00-00-2007**

4. TITLE AND SUBTITLE	5a. CONTRACT NUMBER
Evidence of a gravity wave breaking event and the estimation of the wave characteristics from sodium lidar observation over Fort Collins, CO (41degreesN, 105degreesW)	5b. GRANT NUMBER
	5c. PROGRAM ELEMENT NUMBER
6. AUTHOR(S)	5d. PROJECT NUMBER
	5e. TASK NUMBER
	5f. WORK UNIT NUMBER
7. PERFORMING ORGANIZATION NAME(S) AND ADDRESS(ES) **Naval Postgraduate School,Department of Meteorology,Monterey,CA,93943**	8. PERFORMING ORGANIZATION REPORT NUMBER
9. SPONSORING/MONITORING AGENCY NAME(S) AND ADDRESS(ES)	10. SPONSOR/MONITOR'S ACRONYM(S)
	11. SPONSOR/MONITOR'S REPORT NUMBER(S)

12. DISTRIBUTION/AVAILABILITY STATEMENT
Approved for public release; distribution unlimited

13. SUPPLEMENTARY NOTES

14. ABSTRACT

15. SUBJECT TERMS

16. SECURITY CLASSIFICATION OF:			17. LIMITATION OF ABSTRACT	18. NUMBER OF PAGES	19a. NAME OF RESPONSIBLE PERSON
a. REPORT	b. ABSTRACT	c. THIS PAGE			
unclassified	**unclassified**	**unclassified**	**Same as Report (SAR)**	**5**	

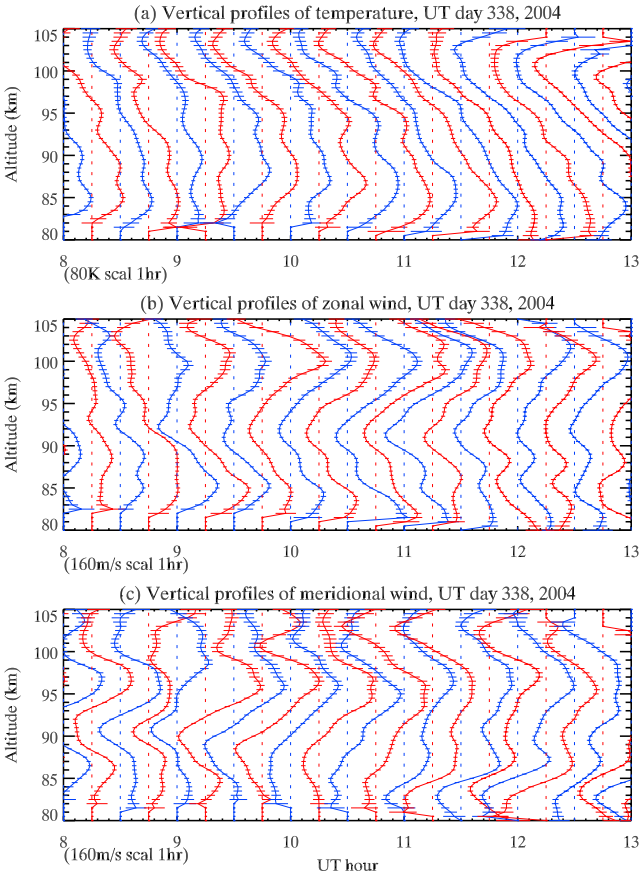

Figure 1. Vertical profiles of (a) temperature, (b) zonal wind, and (c) meridional wind between 0800 and 1300 UT on the night of December 3rd (UT day 338), 2004. These profiles are spaced at 15 min intervals; whose horizontal scale also correspond to 20 K in temperature or 40 m/s in wind speed. The vertical dotted lines denote 200 K for temperature and 0 m/s for wind.

1.5 K and 3 m/s, respectively, at 92 km (sodium peak), and 6 K and 12 m/s, respectively, at both 81 km and 105 km (sodium layer edges).

[5] During our December 2004 campaign, we observed significant horizontal wind acceleration and temperature cooling near 100 km and temperature warming near 96 km between 0900–0915 UT on the night of December 3rd, 2004. The vertical profiles of temperature (a), zonal wind (b), and meridional wind (c), with 15 min temporal resolution and 2 km vertical resolution between 0800 and 1300 UT for this night are shown in Figure 1. These 15-min-averaged profiles are spaced at 15 min interval, which also correspond to 20 K for temperature and 40 m/s for wind. The vertical dotted lines represent 200 K for temperature and 0 m/s for wind. On the temperature plots, we could clearly see that the temperature suddenly warms up near 96 km and cools down near 100 km at around 0900 and 0915 UT. After 0915 UT, this thermal pattern of cooling and heating started to progress downward with a speed of ~1 km/hr. In the zonal and meridional wind components, we saw horizontal wind acceleration near 100 km toward northeast direction at 0900 UT. After 0900 UT, zonal wind remains large in the eastward direction at 100 km for several hours without clear downward progression. The positive peak of meridional wind at ~97 km grew much larger after 0900 UT than the peak at the same altitude before 0900 UT and progressed downward slowly. However, the negative peak below 90 km progressed downward with a faster speed before and after 0900 UT. All these indicate the complexity of wave dynamics during this night.

[6] Shown in the Figure 2 are the plot of zonal wind vs. UT hour at 100 km (left panel) and the contour plots of Lomb power spectra between 0500 and 0900 UT (right top), between 0900 and 1300 UT (right bottom) based on the same dataset shown in Figure 1. The 90% significant level is also plotted in Figure 2 with the white solid lines. As clearly shown in the left panel, the wave oscillation with ~1.5 hr period and ~15 m/s amplitude persists between 0500 and 0900 UT, which is also present in the Lomb power spectrum (right top panel). After 0900 UT, the mean zonal wind increases dramatically, and at the same time the 1.5 hr wave oscillation disappears. The disappearance of this wave is also confirmed in the Lomb power between 0900 and 1300 UT at right bottom panel. Therefore, it is most likely that the temperature warming and mean flow acceleration between 0900 and 0915 UT are due to the breaking of an upward propagating gravity wave with an apparent period of ~1.5 hr. Lomb power spectra of both temperature and meridional wind were similarly examined, the presence and absence of 1.5 hr wave before and after 0900 UT is also evident.

3. Results and Discussion

[7] The Lindzen's linear saturation theory has been the base of most GW parameterization schemes used in both mechanistic and General Circulation global scale Models [e.g. *Holton*, 1982; *Alexander and Dunkerton*, 1999; *Sassi et al.*, 2002], and the applications have been quite successful. It has been compared with mesoscale nonlinear numerical results, and reasonable agreements were found [*Liu et al.*, 1999]. Therefore, we are going to use this theory to estimate the characteristics of breaking gravity wave. According to linear saturation theory, the mean flow accel-

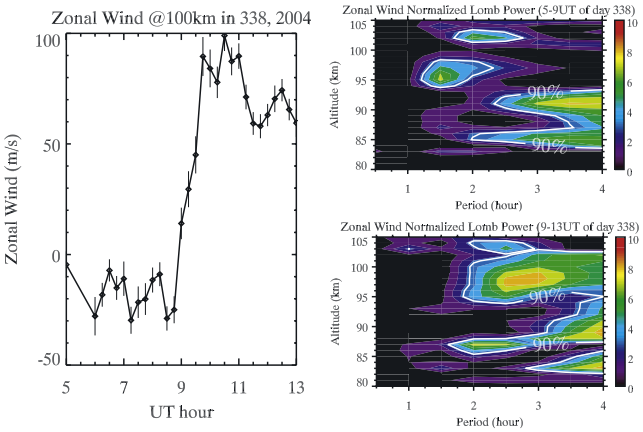

Figure 2. (left) The plot for zonal wind vs. UT hour at 100 km and the contour plots of Lomb power spectra (top right) between 0500 and 0900 UT and (bottom right) between 0900 and 1300 UT. The 90% significant level is also plotted with white lines in the Lomb power contours.

eration in the region where the monochromatic gravity wave breaks is given by [*Holton*, 1982]

$$\frac{\partial \bar{u}}{\partial t}\Big|_{z=z_{break}} = -\frac{1}{\rho_0}\frac{d}{dz}\left(\rho_0\ \overline{u'w'}\right) = \frac{N^2 \bar{K}_m}{(\bar{u}-c)} \tag{1}$$

where ρ_0 is the air density; $\bar{u}$ is horizontal mean wind projected in the wave propagation direction; $\overline{u'w'}$ is the vertical flux of horizontal momentum with u' and w' being perturbations of horizontal wind and vertical wind, respectively; c is horizontal phase speed of the gravity wave (with c-$\bar{u}$ the intrinsic wave phase speed); N is Brunt-Väisällä frequency of the background flow (including tidal components); z is altitude; z_{break} is the altitude where wave breaks; and $\bar{K}_m$ denotes the eddy diffusion coefficient, which is expressed as [*Lindzen*, 1981]:

$$\bar{K}_m = \frac{k(\bar{u}-c)^4}{N^3}\left(\frac{1}{2H} - \frac{3}{2}\frac{1}{\bar{u}-c}\frac{d\bar{u}}{dz}\right) \tag{2}$$

where k is the horizontal wave number; H is the scale height; and $d\bar{u}/dz$ is the vertical shear of horizontal mean wind in the wave propagation direction. Since the gravity wave perturbation is relative to the background atmosphere at break region, there is no explicit wave amplitude information in the equation (1). The maximum heating rate below the breaking region is given by [*Liu*, 2000]

$$\left(\frac{\partial \bar{T}}{\partial t}\right)_{\max |z<z_{break}} = \xi \frac{T_0|_{z=z_{break}}}{g|\lambda_z|\left(1+\frac{|\lambda_z|}{4H}\right)} N^2 \bar{K}_m; \quad with\ \xi \equiv \frac{(3-4\eta)}{P_r} \tag{3}$$

where T_0 is mean temperature over the breaking region; η is a measure of the localization of turbulence; g is the gravitational acceleration; λ_z is the vertical wavelength of the gravity wave; Pr is the Prandtl number. Equation (3) is equation (21) of *Liu* [2000], except where $4-3\eta$ is a typo for the correct factor of $3-4\eta$. Since the observed gravity wave period is ~1.5 hr and much shorter than the inertial period of ~18.5 hr at lidar location, the gravity wave dispersion relation can be simplified to [*Fritts and Alexander*, 2003]

$$|c-\bar{u}| = \frac{N}{|m|} \tag{4}$$

where m is the vertical wave number ($m = 2\pi/\lambda_z$). This equation relates the vertical wave number to the intrinsic phase speed of the wave and the Brunt-Väisällä frequency.

[8] Since the CSU sodium lidar system can simultaneously and continuously observe the vertical profiles of temperature, zonal wind and meridional wind with high temporal and vertical resolutions, we are able to obtain the time derivative of the temperature and horizontal wind, to be used for the left-hand side of equations (1) and (3). The H, $\bar{u}$, and N in equation (1), T_0 in equation (3), and $d\bar{u}/dz$ in equation (2) could be derived from observed background atmosphere before the wave breaking. In fact, if ξ is treated as an adjustable parameter, there are only 4 unknowns (c, k, $\bar{K}_m$, m) in the 4 equations, (1)–(4). Therefore, we can then

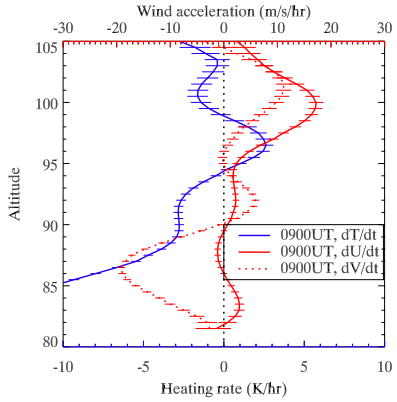

Figure 3. The heating rate, zonal wind acceleration, and meridional wind acceleration at 0900 UT on the night of December 3rd (UT day 338), 2004. The breaking region is near 100 km.

infer the wave characteristics, such as vertical wavelength (λ_z), horizontal wavelength (λ_h), horizontal phase speed (c), and wave period (λ_h/c) as well as the eddy diffusion coefficient ($\bar{K}_m$).

[9] Shown in Figure 3 are the vertical profiles of heating rate, zonal wind acceleration, and meridional wind acceleration of the mean flow at 0900 UT. These profiles were obtained by first smoothing the vertical profiles (Figure 1 but with 4 km vertical resolution to reduce statistical uncertainty) over 1.5 hours and then removing the tidal components of 24 hr, 12 hr, 8 hr, and 6 hr periods prior to the calculation of time derivative, with which the rate of changes between two smoothed profiles at 45 min before and after is evaluated. There exist positive peaks for both zonal wind acceleration and meridional wind acceleration near 100 km with the values of 17 m/s/hr and 11 m/s/hr respectively. The negative peak in heating rate of 1.5 K/hr at 100 km and the positive peak of 2.6 K/hr near 96 km are indicative of downward heat flux associated with wave breaking. The negative peaks below 95 km in the heating rate and meridional wind acceleration are due to wave oscillations, as we saw a clear oscillation below 95 km with downward phase progression in temperature and meridional wind profiles (Figure 1).

[10] Since the onset of wave breaking is near 0900 UT, we use the 1.5 hr smoothed vertical profiles at 0815 UT for the calculation of background atmosphere parameters before wave breaking. The background temperature, zonal wind, meridional wind, Brunt-Väisällä frequency, and mean wind shear at the wave propagation direction near 100 km are 188.3 K, −11.6 m/s, 17.1 m/s, 0.015 s^{-1}, and 0.55 m/s/km, respectively. Using equations (1)–(4), we are able to determine the gravity wave characteristics. However, the wave characteristics along with eddy diffusion coefficient deduced will be sensitive to the choice of the value for ξ in equation (3). By trial and error, it is found that with $\xi = 4$, the apparent wave period determined from equations (1–4) is 85 min, which is close to the 1.5 hr period revealed in Figure 2. Near 100 km at 0900 UT, this gravity wave propagates at ~30° north of east as can be determined by the vector of horizontal wind acceleration. This choice of ξ yields a wave intrinsic period of 79 min, an apparent phase

Table 1. Characteristics of the Breaking Monochromatic Gravity Wave[a]

$\xi = (3-4\eta)/\mathrm{Pr}$	3.5	4.0	4.5
Apparent period, min	36	85	155
Apparent phase speed, m/s	11	20.5	30
Intrinsic period, min	31	79	145
Intrinsic phase speed, m/s	12.6	22.1	31.6
Vertical wavelength, km	5.3	9.4	13.5
Horizontal wavelength, km	24	105	278
Eddy diffusion coefficient, m^2/s	315	550	790

[a]Horizontal wave propagation direction: 30° North of East.

speed of 20.5 m/s (22.1 m/s intrinsic), vertical wavelength of 9.4 km, and horizontal wavelength of 105 km. To examine the sensitivity of the solutions to ξ, we also solve the equations with ξ = 3.5 and 4.5 and the results are given in Table 1. The apparent wave periods in these two cases were determined to be 36 min and 155 min respectively, different from the observed period of 1.5 hr.

[11] For the 3 choices of ξ (3.5, 4.0, and 4.5), the deduced eddy viscosities are, respectively, 315, 550, and 790 m^2/s. In view of its variability, these are all consistent with the average value of 320 m^2s^{-1} determined from the momentum flux measurements by sodium lidar [*Gardner and Yang*, 1998]. The choice of ξ = 4.0 provides a constraint on the Prandtl number and turbulence localization measure: $3-4\eta = 4$ Pr. If we assume isotropic turbulence (η = 0), then the Pr number should be 0.75, and if η = 0.25, then Pr = 0.5. For the onset of the gravity wave breaking and turbulence, these values of η and Pr are plausible. Using the value of ξ = 4.0 and observed background temperature and scale height, we can calculate, as an independent check, the cooling rate due to wave breaking from equation (20) of *Liu* [2000], which resulted in ~1.9 K/hr, consistent with the observed value at 100 km in Figure 3.

[12] To extract amplitudes and phases of this gravity wave packet with a period of 1.5 hr from observation, we performed a linear least-square fit with mean plus 1.5 hr period wave on the raw dataset between 0600 and 0900 UT, yielding the best-fit vertical profiles of amplitudes and phases. By visually examining the fitting, we are confident about the fitting results. The vertical wavelength derived from phase plots is about 10–15 km, which is consistent with the estimation of the middle column in Table 1. The temperature, zonal wind, and meridional wind amplitudes were determined to be ~5 K, 10–15 m/s, and 10–15 m/s respectively, near 100 km. The horizontal wind amplitude is thus obtained to be ~15–21 m/s, which is close to the wave intrinsic phase speed of ~22 m/s. This lends further support for the saturation of the 1.5 hr gravity wave via convective instability near 100 km, since the linear theory suggests the horizontal wind perturbation is equal to the wave intrinsic phase speed when the wave becomes convectively unstable [*Fritts and Alexander*, 2003].

[13] Shown in the Figure 4 are the vertical profiles of Brunt-Väisällä frequency square (N^2) and Richardson number (Ri) between 0800 and 1300 UT based on the same dataset shown in Figure 1. These profiles are spaced at 15 min intervals, whose horizontal scale correspond to $5 \times 10^{-4}s^{-2}$ in N^2 or 3 in Ri. The vertical dotted lines denote the instability threshold corresponding to 0 for N^2 or 0.25 for Ri. Within the error bar indicated, the dynamic instability threshold of 0.25 may have been reached at 0815 UT near 100 km and the convective instability threshold of 0 was then reached at both 0830 and 0845 UT. When the significant changes of both temperature and horizontal wind were found near 0900 UT (Figures 1 and 3), however, the N^2 and Ri near 100 km are 1.0×10^{-4} s^{-2} and 0.7 respectively. The 1.5 hr period gravity wave could start to break after 0845 UT, and then the turbulence mixing locally generated within the breaking gravity wave field could bring the lapse rate to adiabatic value and make the atmosphere more stable. The acceleration due to wave breaking will increase the shear below the wave breaking zone and in turn cause secondary instability [*Liu et al.*, 1999; *Fritts and Alexander*, 2003]. At 0915 UT, the N^2 was observed to be more negative near 98 km and wind shear is also dramatically increased. After 9:15 UT, atmospheric layers near convective or dynamic instability developed below 100 km, with lower boundary starting at ~98 km at 9:15 UT progressing downward with a speed of ~1 km/hr, in agreement with tidal phase propagation during this time period of 2 to 3 hours. The time series in Figure 4 is consistent with initial wave breaking near 0900 UT via convective instability, which then trigger and influence the subsequent instability and mixing [*Fritts and Alexander*, 2003]; this lasted until ~1200 UT in a manner similar to secondary instability under strong shear condition investigated by *Isler et al.* [1994].

4. Conclusion

[14] On the night of December 3rd, 2004, the Colorado State University sodium lidar system at Fort Collins, CO

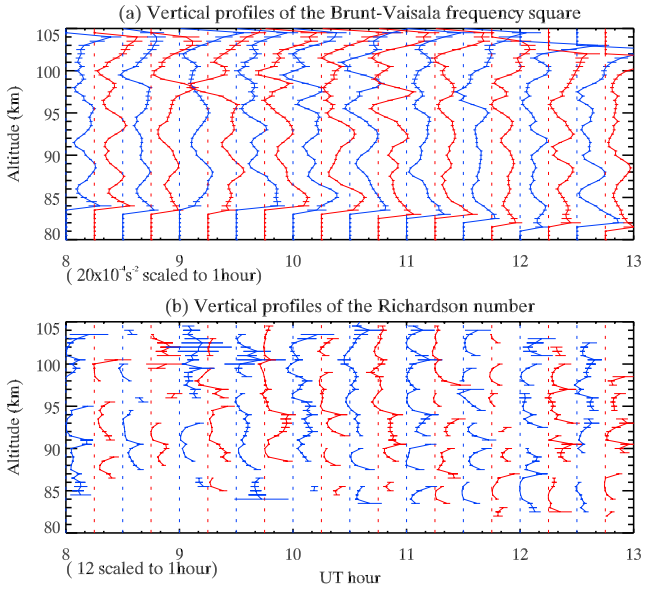

Figure 4. Vertical profiles of (a) Brunt-Väisällä frequency square and (b) Richardson number between 0800 and 1300 UT on the night of December 3rd (UT day 338), 2004. These profiles are spaced at 15 min intervals, whose horizontal scale also corresponds to $5 \times 10^{-4}s^{-2}$ in Brunt-Väisällä frequency square or 3 in Richardson number. The vertical dotted lines denote the instability threshold corresponding to 0 for Brunt-Väisällä frequency square or 0.25 for Richardson number.

observed significant horizontal wind acceleration near 100 km accompanied by a temperature cooling at the same altitude and a temperature warming near 96 km between 0900–0915 UT. This phenomenon is consistent with the modeling prediction for the interaction between gravity wave and mean flow. Employing the gravity wave linear saturation theory and dispersion relation, we deduced realistic values for eddy viscosity as well as breaking wave characteristics from the observed heating rate, horizontal wind acceleration, and background atmosphere without invoking modeling simulation. By approximately equating the calculated wave period to the observed apparent period, we determined the simple relation between Prandtl number and turbulence localization measure imposed by the linear saturation theory.

[15] The 1.5 hr period oscillation at 100 km is clearly seen in the zonal wind component before 0900 UT, but not after 0900 UT. The Lomb spectrum analysis also showed the similar scenario that the power of gravity wave with 1.5 hr period is strong with above 90% confidence level between 0500 and 0900 UT, but very weak between 0900 and 1300 UT, indicating the wave saturation or breaking. The horizontal wind amplitude deduced from observation is ~15–21 m/s, which is close to the wave intrinsic phase speed of ~22 m/s. The averaged vertical wavelength determined from vertical phase plot is consistent with the estimation from the linear saturation wave theory. Therefore, it is most likely that the temperature warming and mean flow acceleration between 0900–0915 UT are due to the breaking of an upward propagating gravity wave with an apparent period of ~1.5 hr. The instability analysis reveals that the 1.5 hr gravity wave could start to break down after 0845 UT via convective instability, and then wave breaking may cause the subsequent instability and mixing after 0915 UT, in a manner indicative of secondary instability under strong shear condition.

[16] To our knowledge, this may very well be the first study, using observed simultaneous temperature and horizontal wind profiles not only to reveal the presence of wave breaking, but also to estimate the characteristics of the breaking wave and the coefficient of eddy viscosity. As such, we have demonstrated the power of simultaneous and continuous observations of temperature and horizontal wind with good temporal and vertical resolutions, by instrument such as the Colorado State University sodium lidar, for the study of wave breaking in the mesopause region of the atmosphere. Studies of this type will be further enhanced by accompanying modeling on the one hand, and by concurrent imager observations on the other to provide the horizontal characteristics of the breaking wave, checking the horizontal wavelength deduced from the linear saturation theory.

[17] **Acknowledgments.** This work done at Colorado State University is supported in part by grants from National Aeronautics and Space Administration, NAG5-10076, and from National Science Foundation, ATM-00-03171 and ATM-0545221. The National Center for Atmospheric Research is supported by the National Science Foundation. The authors acknowledge the contribution of Phil Acott, Biff Williams, Tao Yuan, and Jia Yue for data acquisition in the December 2004 campaign.

References

Alexander, M. J., and T. J. Dunkerton (1999), A spectral parameterization of mean-flow forcing due to breaking gravity waves, *J. Atmos. Sci.*, *56*, 4167–4182.

Fritts, D. C., and M. J. Alexander (2003), Gravity wave dynamics and effects in the middle atmosphere, *Rev. Geophys.*, *41*(1), 1003, doi:10.1029/2001RG000106.

Fritts, D. C., and P. K. Rastogi (1985), Convective and dynamical instabilities due to gravity wave motions in the lower and middle atmosphere: Theory and observations, *Radio Sci.*, *20*, 1247–1277.

Gardner, C. S., and W. Yang (1998), Measurement of the dynamical cooling rate associated with the vertical transport of heat by dissipating gravity waves in the mesopause region at the Starfire Optical Range, New Mexico, *J. Geophys. Res.*, *103*, 16,909–16,926.

Hauchecorne, A., M. L. Chanin, and R. Wilson (1987), Mesopheric temperature inversion and gravity wave breaking, *Geophys. Res. Lett.*, *14*, 933–936.

Hines, C. O. (1960), Internal atmospheric gravity waves at ionospheric heights, *Can. J. Phys.*, *38*, 1441–1481.

Holton, J. R. (1982), The role of gravity wave induced drag and diffusion in the momentum budget of the mesosphere, *J. Atmos. Sci.*, *39*, 791–799.

Isler, J. R., D. C. Fritts, Ø. Andreassen, and C. E. Wasberg (1994), Gravity wave breaking in two and three dimensions: 3. Vortex breakdown and transition to isotropy, *J. Geophys. Res.*, *99*, 8125–8138.

Li, T., C. Y. She, B. P. Williams, T. Yuan, R. L. Collins, L. M. Kieffaber, and A. W. Peterson (2005), Concurrent OH imager and sodium temperature/wind lidar observation of localized ripples over northern Colorado, *J. Geophys. Res.*, *110*, D13110, doi:10.1029/2004JD004885.

Lindzen, R. S. (1981), Turbulence and stress owing to gravity wave and tidal breakdown, *J. Geophys. Res.*, *86*, 9707–9714.

Liu, H.-L. (2000), Temperature changes due to gravity wave saturation, *J. Geophys. Res.*, *105*, 12,329–12,336.

Liu, H.-L., and M. E. Hagan (1998), Local heating/cooling of the mesosphere due to gravity wave and tidal coupling, *Geophys. Res. Lett.*, *25*, 2941–2944.

Liu, H.-L., P. B. Hays, and R. G. Roble (1999), A numerical study of gravity wave breaking and impacts on turbulence and mean state, *J. Atmos. Sci.*, *56*, 2152–2177.

Meriwether, J. W., X. Gao, V. B. Wickwar, T. Wilkerson, K. Beissner, S. Collins, and M. E. Hagan (1998), Observed coupling of the mesosphere inversion layer to the thermal tidal structure, *Geophys. Res. Lett.*, *25*, 1479–1482.

Sassi, F., R. R. Garcia, B. A. Boville, and H. Liu (2002), On temperature inversions and the mesospheric surf zone, *J. Geophys. Res.*, *107*(D19), 4380, doi:10.1029/2001JD001525.

She, C. Y., et al. (2004), Tidal perturbations and variability in the mesopause region over Fort Collins, CO (41 N, 105 W): Continuous multi-day temperature and wind lidar observations, *Geophys. Res. Lett.*, *31*, L24111, doi:10.1029/2004GL021165.

Williams, B. P., M. A. White, D. A. Krueger, and C. Y. She (2002), Observation of a large amplitude wave and inversion layer leading to convective instability in the mesopause region over Fort Collins, CO (41°N, 105°W), *Geophys. Res. Lett.*, *29*(17), 1850, doi:10.1029/2001GL014514.

T. Li, Table Mountain Facility, Jet Propulsion Laboratory, California Institute of Technology, 24490 Table Mountain Road, PO Box 367, Wrightwood, CA 92397, USA. (taoli@tmf.jpl.nasa.gov)

H.-L. Liu, High Altitude Observatory, National Center for Atmospheric Research, Boulder, CO 80307-3000, USA.

M. T. Montgomery, Department of Meteorology, Naval Postgraduate School, Monterey, CA 93943, USA.

C.-Y. She, Department of Physics, Colorado State University, Fort Collins, CO 80523-1875, USA.